Minimum Energy Paths for Non-Adiabatic Charge Transitions in Oxide Defects

D. Waldhoer[1,2], Y. Wimmer[2], A.-M. El-Sayed[1,3], W. Goes[2], M. Waltl[1,2], and T. Grasser[2]
[1]*Christian Doppler Laboratory for Single-Defect Spectroscopy* at the
[2]*Institute for Microelectronics, TU Wien*, A-1040 Vienna, Austria
[3]*Nanolayers Research Computing Ltd*, London, United Kingdom
E-mail: waldhoer@iue.tuwien.ac.at

***Abstract*—Charge transfer between oxide defects and device substrate can be described as a non-radiative multiphonon transition. Within this approach oxide defects are usually modelled as 1-dimensional harmonic oscillators. In the classical limit the charge transition dynamics are determined by the crossing point of the corresponding diabatic potential energy curves of the defects. In this work we go beyond the harmonic approximation and present a scheme to locate the minimum energy path between two differently charged defect configurations on multidimensional potential energy surfaces obtained with density functional theory. Using this more accurate method we quantify the accuracy of the harmonic approximation and demonstrate its applicability for common defects in amorphous silica. Furthermore, we compare the resulting transition barriers with experimental data and demonstrate excellent agreement for hydrogen-related defect species.**

***Index Terms*—BTI, RTN, DFT, oxide defects, charge trapping, nonradiative multiphonon (NMP) theory**

I. Introduction

We focus on hole trapping in oxide defects which significantly changes the device electrostatics. This mechanism is believed to be at the core of negative bias temperature instability [1], [2] (NBTI) and random telegraph noise [3] (RTN) in pMOS devices with a SiO_2 dielectric. For a given atomistic defect model charge transfer between defect and substrate can be studied by combining density functional theory (DFT) with the non-radiative multiphonon (NMP) model for non-adiabatic charge transitions [4]. Within this model the so-called harmonic approximation (HA) is frequently employed. Here the different charge states of a defect are treated as 1D harmonic oscillators and are therefore represented by parabolic potential energy curves $V_i(q)$ along a configuration coordinate q as shown in Fig. 1. The classical capture and emission barriers, denoted by ε_{12} and ε_{21} respectively, are then determined by the crossing point (CP) of these energy curves. Note that an applied gate bias shifts the energy curves relative to each other by ΔS, resulting in bias dependent charge transition barriers. Each parabola is linked to a physical defect model by two fitting points, which are obtained from DFT energy calculations for each charge state. These points are indicated by the circles in Fig. 1. However, as can be also seen here, the relevant CP usually does not lie near these physical fitting points. It is therefore possible that the harmonic approximation fails to give accurate estimates for the crossing point energy and the resulting classical barriers. This uncertainty in barrier heights can lead to errors in transition rate predictions by several orders of magnitude. In this work we overcome this problem by calculating the dominant transition path directly in the multidimensional configuration space instead of a 1D representation. We will apply this method to frequently studied defect candidates for NBTI in amorphous silica (a-SiO_2), namely the oxygen vacancy [5] (OV), the hydrogen bridge [6] (HB) and the hydroxyl-E′ center [7] (H-E′). A schematic illustration of the studied defects is provided in Fig. 2. We use the resulting charge transition barriers obtained with this method as a benchmark for the accuracy of the HA. The obtained theoretical barriers for the aforementioned defect candidates are then compared to experimental values for devices with an a-SiO_2 dielectric.

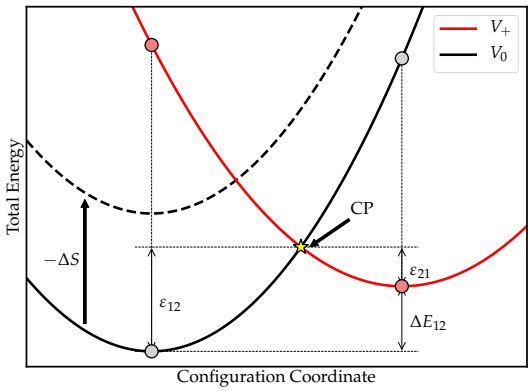

Fig. 1. Schematic illustration of the harmonic approximation often used in NMP theory. The potential energy curves are parabolas, which are fitted to DFT energies at the points indicated by the 4 circles. In the classical limit the transition rates are determined by the barriers ε_{12} and ε_{21} with respect to the classical crossing point (CP). The solid black line represents the neutral defect in flatband conditions. An applied gate bias shifts the neutral energy curve of the defect by ΔS [1], resulting in the dashed line. The capture and emission barriers are thus bias dependent.

The research leading to this work has been funded by the Christian Doppler Laboratory (CDL) for Single Defect Spectroscopy, by RELTMD (FWF - No. I2606-N30), by Austrian Science Fund grand No. 496246 as well as Take-Off programs of FFG (INNAS - 867414; INCAE - 861022). Computational resources were provided by the Vienna Scientific Cluster.

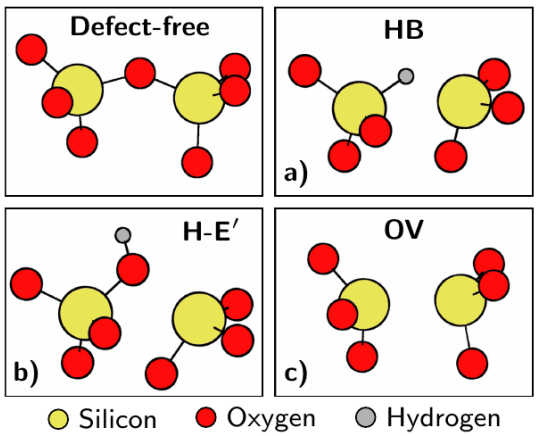

Fig. 2. Atomic configurations of the studied defect types in their neutral charge state. The hydrogen bridge (HB) forms if an oxygen atom is replaced by hydrogen **(a)**. In the case of the hydroxyl-E′ center (H-E′) a H atom is bound to the O atom, breaking one of the Si-O bonds in its neutral charge state **(b)**. The oxygen vacancy (OV) forms if an oxygen atom is missing **(c)**.

II. Minimum Energy Path

Instead of the simple 1D energy curves used in the HA we now use the full potential energy surfaces (PESs) $V_i\left[\boldsymbol{r}\right]$ as a function of all atomic coordinates $\boldsymbol{r}$. For a system of N atoms, the PES intersection is not a single point in configuration space, but a multidimensional surface, the so-called seam. Since charge transitions obey an exponential Arrhenius law [3], the point in the seam with lowest energy, known as minimum energy crossing point (MECP), dominates the total transition rates. The situation is illustrated in Fig. 3 for a system with two degrees of freedom and a one dimensional seam.

Constructing the minimum energy path (MEP) between the two defect states (minima of the PESs) can be split into two separate tasks. First, the MECP is located inside the seam with an optimization scheme (see below). In a second step both minima are connected to the MECP using the improved tangent nudged elastic band (IT-NEB) algorithm [8]. This results in two individual path segments which join smoothly at the MECP. The MECP itself can be extracted from DFT calculations by solving the following constrained optimization problem:

$$\text{minimize} \quad F\left(\boldsymbol{r}\right) \coloneqq V_0^{\mathrm{DFT}}\left[\boldsymbol{r}\right] + V_+^{\mathrm{DFT}}\left[\boldsymbol{r}\right] \tag{1a}$$

$$\text{subject to} \quad C\left(\boldsymbol{r}\right) \coloneqq V_0^{\mathrm{DFT}}\left[\boldsymbol{r}\right] - V_+^{\mathrm{DFT}}\left[\boldsymbol{r}\right] \stackrel{!}{=} 0 \tag{1b}$$

The applied constraint $C\left(\boldsymbol{r}\right) = 0$ ensures an optimization of the cost function $F\left(\boldsymbol{r}\right)$ within the seam of the two surfaces. Although it would be sufficient to choose either $V_0^{\mathrm{DFT}}\left[\boldsymbol{r}\right]$ or $V_+^{\mathrm{DFT}}\left[\boldsymbol{r}\right]$ as cost function, it was demonstrated that the stability of the optimization scheme is significantly improved [9] by using the combined cost function $F\left(\boldsymbol{r}\right)$.

III. Simulation Framework

The amorphous structure of the gate oxide leads to a wide range of experimentally observed defect parameters. In order

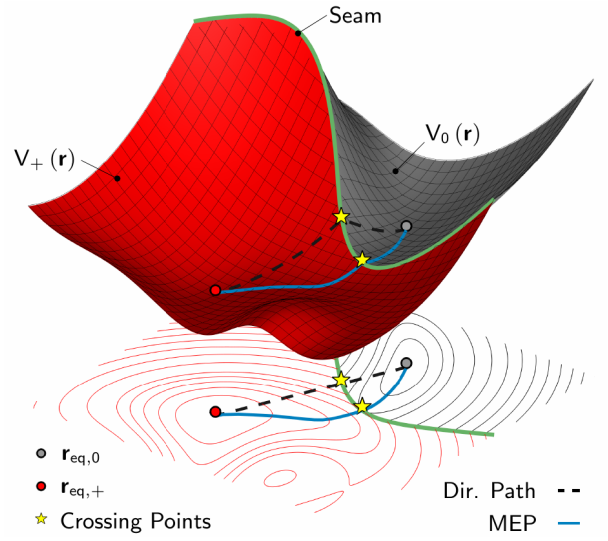

Fig. 3. Transition between two schematic diabatic PESs with two possible reaction paths marked. The minimum energy path (MEP) **(blue)** connects the two PESs across the minimum energy crossing point (MECP). Every other path, including the direct one **(black)**, overestimates the transition barriers.

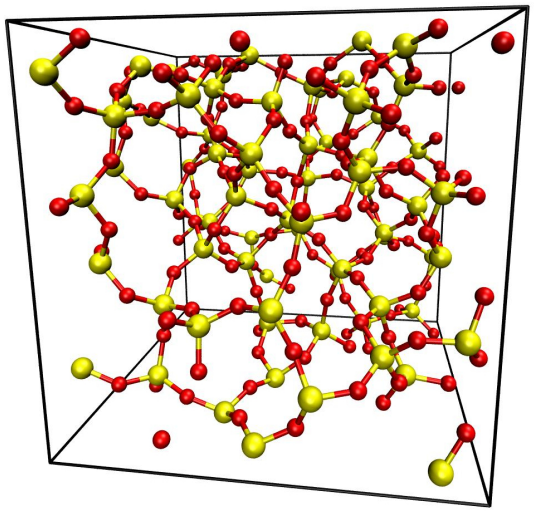

Fig. 4. An a-SiO_2 model structure used in this work as a host for defects. The amorphous model contains 216 atoms and is enclosed in a cubic simulation cell with periodic boundary conditions and a side length of 15 Å.

to capture the statistical defect properties in our simulations, we performed all calculations in amorphous SiO_2 models. We employed the melt-and-quench technique together with the empirical force-field ReaxFF [10] to melt and rapidly cool a $2 \times 2 \times 2$ supercell of β-cristobalite in order to create a-SiO_2 models. This specific polymorph of crystalline silica was used as a starting point since it matches the density of deposited SiO_2 films on silicon (2.2 g/cm^3) [11]. The resulting defect-free a-SiO_2 structures consist of 216 atoms and are contained in a simulation cell with periodic boundary conditions in order to mimic a bulk oxide. A typical structure used in this work is depicted in Fig. 4.

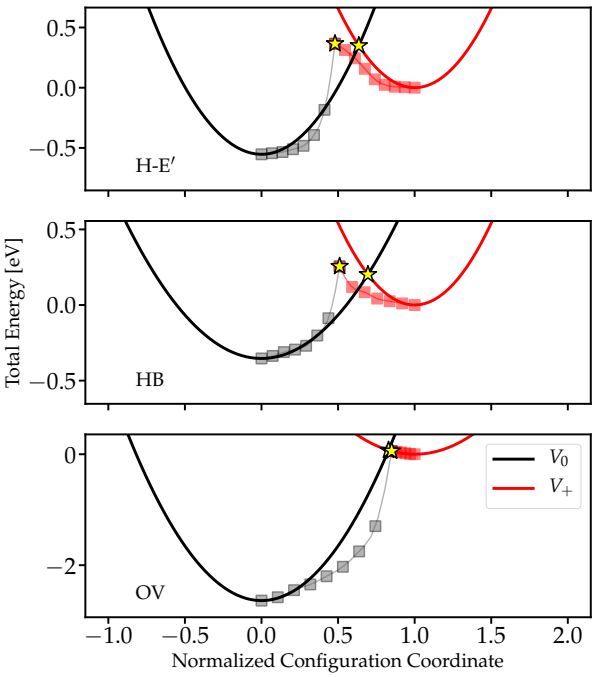

Fig. 5. Resulting energy curves of the HA **(solid)** and MEP **(dots)** method for a representative defect of each kind at $\Delta S = 0.0$ eV. The crossing point energy is reproduced well by the HA for all three defects. However, the shape of the MEP energy curve significantly differs from a parabolic shape.

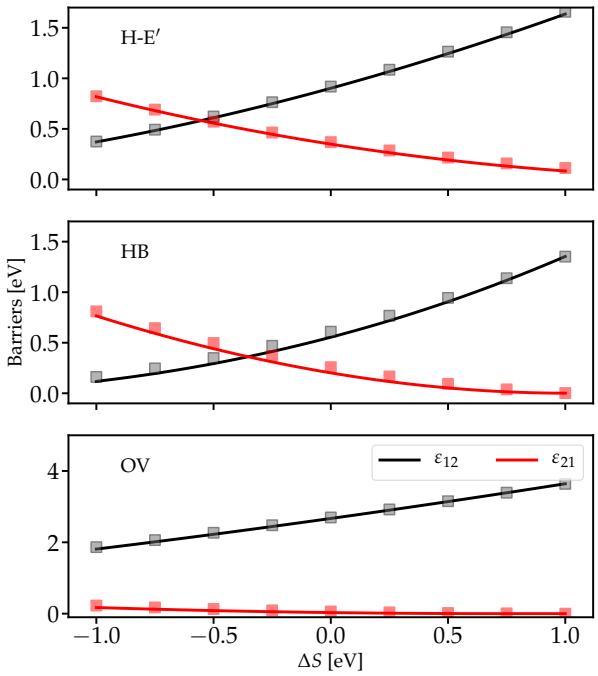

Fig. 6. Capture and emission barriers, denoted ε_{12} and ε_{21} respectively, as a function of the shift ΔS for the same defects as in Fig. 5. The HA **(solid)** performs nicely in reproducing the bias dependency of the barriers from the MEP method **(dots)**. The hydrogen-related defects show a switching of their thermodynamically stable charge state at around $\Delta S \approx -0.5$ eV, which is reachable under typical operating conditions of a pMOS. In contrast, the OV remains neutral for all relevant bias conditions in thin oxides.

We used the CP2K [12] DFT code together with the PBE0 TC LRC hybrid functional [13] and a plane-wave cutoff of 400 Ry to further relax the amorphous structures. Defects were inserted manually and their equilibrium geometries and formation energies were obtained with DFT. In this work we studied 27 H-E′ centers, 11 HBs and 14 OVs.

For every defect the barriers within the HA and along the MEP were calculated with DFT. The MEP search was realized by coupling an external Python script to the DFT code. The external optimizer determines a search direction based on the DFT potential energies $V_i(\boldsymbol{r})$ as well as the corresponding gradients ∇V_i of both charge states. The sequential quadratic programming [14] (SQP) optimization algorithm as implemented in the SciPy package is used to solve Eq. 1. The CP obtained by linear interpolation as shown in Fig. 3 was used as initial guess for the optimizer since it represents an easily obtainable point of the seam. The energy curves and barriers along the MEP serve as a reference to assess the quality of the much simpler HA.

IV. Results and Discussion

We start by discussing a representative defect of each kind. Fig. 5 shows the resulting energy curves for the HA and along the MEP for a fixed gate bias $\Delta \mathrm{S} = 0.0$ eV. As can be seen, the HA can predict the MECP energy, and subsequently the transition barriers for hole capture and emission, quite accurately for all three defect types. On the other hand, the shape of the energy curves is not well reproduced. Surprisingly, this does not affect the accuracy for the bias dependencies of ε_{12} and ε_{21}, which still show a good agreement between HA and MEP as demonstrated in Fig. 6. These findings also hold true when considering a whole ensemble of defects in order to account for the statistical distribution of defect parameters in the amorphous gate oxide. The plots presented in Fig. 7 show the correlation between barriers obtained with the HA and the MEP for various gate biases. In these plots a perfect approximation would lie along the drawn diagonal. As can be seen, the deviations are largest for the H-E′ center defects. This result is expected since the defect structure is more complicated compared to the OV and HB defects leading to a longer transition path in configuration space. However, in all studied cases the error from using the HA is clearly small compared to the intrinsic spreading of barrier heights introduced by the amorphous oxide. Fig. 7 also shows that a significant portion of hydrogen-related defects lies within the experimentally accessible range of barriers and thus can contribute to NBTI degradation, whereas the OVs will remain mostly inactive. This finding agrees with previous theoretical studies [15]–[17] on a-SiO_2 defects. It should be noted that the OV defect can still charge when sufficiently thick oxides are used which allow for larger possible values for ΔS under realistic bias conditions. However, in modern devices with thin oxid layers the achievable shift is too small to activate OV defects based on these results.

The above findings validate the treatment of oxide defects in SiO_2 using the HA in reliability models. Typi-

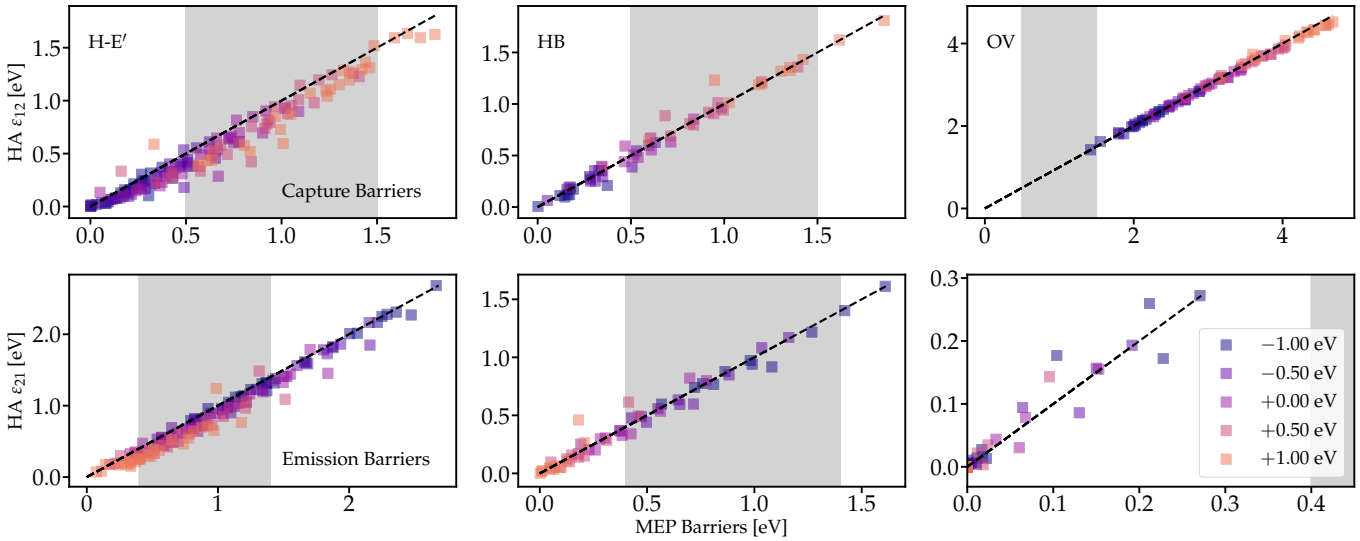

Fig. 7. Correlation plots showing the agreement for capture **(top)** and emission **(bottom)** barriers between HA and MEP for various bias conditions ΔS. The dashed lines indicate a perfect match. As can be seen, the HA gives surprisingly good results for all defects and bias conditions. The error introduced by this approximation is always small compared to the parameter spreading due to the amorphous structure. The shaded areas mark the region [15] which is experimentally accessible.

cally the parabolic potential energy curves of the defect are parametrized by the relaxation energy S and the curvature ratio R. The capture and emission barriers are linked to these parameters by [3]

$$\varepsilon_{12} = \frac{S}{(R^2-1)^2}\left(1 - R\sqrt{\frac{S + \Delta E_{12}(R^2-1)}{S}}\right)^2 \tag{2a}$$

$$\varepsilon_{21} = \varepsilon_{12} - \Delta E_{12} \tag{2b}$$

where ΔE_{12} is the relative energetic position of the two defect states as shown in Fig. 1.

Such a model is implemented in the compact physics framework Comphy [18], which allows the experimental extraction of (R, S), and subsequently the barriers $(\varepsilon_{12}, \varepsilon_{21})$, from extended measure-stress-measure (eMSM) sequences. We used the extracted parameters for the hole trap band in the *SiON 28nm foundry planar* technology node and compared the resulting barriers to the results obtained with the MEP method. In Fig. 8 one can see an excellent agreement between the predictions for hydrogen-related defects and the experimental data, reinforcing the validity of the NMP model and the role of the HB and H-E′ defects in NBTI degradation.

V. Conclusions

We have presented a feasible strategy for finding the minimum energy path for charge transitions in oxide defects from first principles. We used this accurate method to test the frequently employed harmonic approximation. We found that this approximation performs well for the studied oxide defects and reproduces important quantities like transition barriers and bias dependencies accurately. Furthermore the theoretical barriers for hydrogen-related defects were found to be in good agreement with experimental NBTI data.

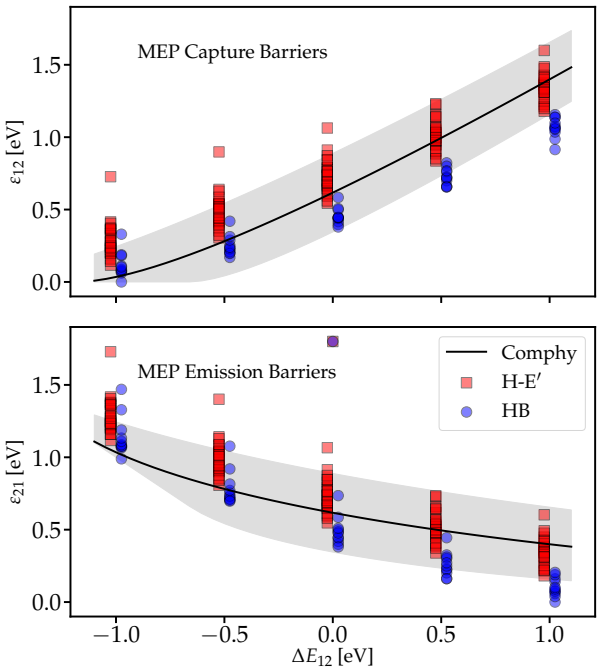

Fig. 8. Comparison between experimental charge transition barriers and theoretical barriers of hydrogen-related defects in a-SiO_2. The experimental data was obtained from Comphy [18] fitting parameters for the extracted hole trap band. The solid line indicates the mean barriers, whereas the shaded area represents the possible barriers within $\pm 1\sigma$ of the experimental parameter distribution. It is demonstrated that the transition barriers of HB and H-E′ defects lie well within the experimental range. Note that the barriers are plotted against the total energy difference ΔE_{12} between the two defect states and not ΔS. This allows us to eliminate additional uncertainties due to trap level and trap position distributions.

REFERENCES

[1] T. Grasser, *Bias temperature instability for devices and circuits*. New York: Springer, 2014.

[2] J. H. Stathis, S. Mahapatra, and T. Grasser, "Controversial issues in negative bias temperature instability," *Microelectronics Reliability*, vol. 81, pp. 244 – 251, 2018. [Online]. Available: http://www.sciencedirect.com/science/article/pii/S0026271417305991

[3] T. Grasser, "Stochastic charge trapping in oxides: From random telegraph noise to bias temperature instabilities," *Microelectronics Reliability*, vol. 52, no. 1, pp. 39 – 70, 2012. [Online]. Available: http://www.sciencedirect.com/science/article/pii/S0026271411004203

[4] F. Schanovsky, W. Goes, and T. Grasser, "An advanced description of oxide traps in MOS transistors and its relation to DFT," *Journal of Computational Electronics*, vol. 9, no. 3, pp. 135–140, Dec 2010. [Online]. Available: https://doi.org/10.1007/s10825-010-0323-x

[5] K. L. Yip and W. B. Fowler, "Electronic structure of E_1' centers in SiO_2," *Phys. Rev. B*, vol. 11, pp. 2327–2338, Mar 1975. [Online]. Available: https://link.aps.org/doi/10.1103/PhysRevB.11.2327

[6] P. E. Blöchl, "First-principles calculations of defects in oxygen-deficient silica exposed to hydrogen," *Phys. Rev. B*, vol. 62, pp. 6158–6179, Sep 2000. [Online]. Available: https://link.aps.org/doi/10.1103/PhysRevB.62.6158

[7] A.-M. El-Sayed, M. B. Watkins, T. Grasser, V. V. Afanas'ev, and A. L. Shluger, "Hydrogen-induced rupture of strained Si-O bonds in amorphous silicon dioxide," *Phys. Rev. Lett.*, vol. 114, p. 115503, Mar 2015. [Online]. Available: https://link.aps.org/doi/10.1103/PhysRevLett.114.115503

[8] G. Henkelman and H. Jonsson, "Improved tangent estimate in the nudged elastic band method for finding minimum energy paths and saddle points," *The Journal of Chemical Physics*, vol. 113, no. 22, pp. 9978–9985, 2000. [Online]. Available: https://doi.org/10.1063/1.1323224

[9] T. Chachiyo and J. H. Rodriguez, "A direct method for locating minimum-energy crossing points (MECPs) in spin-forbidden transitions and nonadiabatic reactions," *The Journal of Chemical Physics*, vol. 123, no. 9, p. 094711, 2005. [Online]. Available: https://doi.org/10.1063/1.2007708

[10] T. P. Senftle, S. Hong, M. M. Islam, S. B. Kylasa, Y. Zheng, Y. K. Shin, C. Junkermeier, R. Engel-Herbert, M. J. Janik, H. M. Aktulga, T. Verstraelen, A. Grama, and A. C. T. van Duin, "The ReaxFF reactive force-field: development, applications and future directions," *npj Computational Materials*, vol. 2, p. 15011 EP, Mar 2016. [Online]. Available: https://doi.org/10.1038/npjcompumats.2015.11

[11] A.-M. El-Sayed, "Atomistic modelling of charge trapping defects in silicon dioxide," PhD Thesis, University Collge London, 2015.

[12] J. Hutter, M. Iannuzzi, F. Schiffmann, and J. VandeVondele, "CP2K: Atomistic simulations of condensed matter systems," *Wiley Interdisciplinary Reviews: Computational Molecular Science*, vol. 4, no. 1, pp. 15–25, 2014. [Online]. Available: https://onlinelibrary.wiley.com/doi/abs/10.1002/wcms.1159

[13] M. Guidon, J. Hutter, and J. VandeVondele, "Auxiliary density matrix methods for HartreeFock exchange calculations," *Journal of Chemical Theory and Computation*, vol. 6, no. 8, pp. 2348–2364, 2010. [Online]. Available: https://doi.org/10.1021/ct1002225

[14] D. Kraft, "A software package for sequential quadratic programming," *Deutsche Forschungs- und Versuchsanstalt für Luft- und Raumfahrt*, 1988, Report.

[15] T. Grasser, W. Goes, Y. Wimmer, F. Schanovsky, G. Rzepa, M. Waltl, K. Rott, H. Reisinger, V. V. Afanas'ev, A. Stesmans, A.-M. El-Sayed, and A. L. Shluger, "On the microscopic structure of hole traps in pMOSFETs," in *2014 IEEE International Electron Devices Meeting*, Dec 2014, pp. 21.1.1–21.1.4.

[16] Y. Wimmer, A.-M. El-Sayed, W. Goes, T. Grasser, and A. L. Shluger, "Role of hydrogen in volatile behaviour of defects in SiO_2-based electronic devices," *Proceedings of the Royal Society A: Mathematical, Physical and Engineering Sciences*, vol. 472, no. 2190, p. 20160009, 2016. [Online]. Available: https://royalsocietypublishing.org/doi/abs/10.1098/rspa.2016.0009

[17] W. Goes, Y. Wimmer, A.-M. El-Sayed, G. Rzepa, M. Jech, A. Shluger, and T. Grasser, "Identification of oxide defects in semiconductor devices: A systematic approach linking DFT to rate equations and experimental evidence," *Microelectronics Reliability*, vol. 87, pp. 286 – 320, 2018. [Online]. Available: http://www.sciencedirect.com/science/article/pii/S0026271417305796

[18] G. Rzepa, J. Franco, B. O'Sullivan, A. Subirats, M. Simicic, G. Hellings, P. Weckx, M. Jech, T. Knobloch, M. Waltl, P. Roussel, D. Linten, B. Kaczer, and T. Grasser, "Comphy - A compact-physics framework for unified modeling of BTI," *Microelectronics Reliability*, vol. 85, pp. 49 – 65, 2018. [Online]. Available: http://www.sciencedirect.com/science/article/pii/S0026271418301641